

Bayesian Parameter Estimation for Predictive Modeling of Illumination-Dependent Current-Voltage Curves

*Eunchi Kim**, *Thomas Kirchartz**

Affiliations

E. Kim, T. Kirchartz
IMD3-Photovoltaik
Forschungszentrum Jülich
52425 Jülich, Germany
E-mail: e.kim@fz-juelich.de
E-mail: t.kirchartz@fz-juelich.de
T. Kirchartz
Faculty of Engineering and CENIDE
University of Duisburg-Essen
Carl-Benz-Str. 199, 47057 Duisburg, Germany

Keywords

machine learning, organic photovoltaics, Bayesian inference, device modeling, high-throughput

Abstract

Machine learning enables rapid estimation of material parameters in solar cells via neural-network-based surrogate models. However, the reliability of extracted parameters depends on underlying assumptions such as the choice of one-dimensional drift-diffusion model and selection of free material parameters. To validate the inferred parameters, we perform predictive modeling of light-intensity-dependent current-voltage (JV) characteristics. Well-known physical effects, including the influence of external resistance and recombination dynamics on illumination-dependent device performance, are reflected in parameter estimation and prediction workflow. We show that correct treatment of dark shunt resistance and emphasizing shifted current ($J + J_{sc}$) during fitting enhances prediction accuracy at low to intermediate illumination level. Additionally, we analyze the information content of various input JV curve combinations, demonstrating that including at least one illuminated JV , preferably not under high illumination due to series resistance effects, is critical for reliable parameter estimation and device performance prediction.

Main

As interest in self-driving laboratories continues to grow for accelerating material discovery^[1-10] and device optimization^[11-17], the accurate identification of material parameters becomes increasingly important. These parameters can serve as essential inputs for feedback algorithms that guide the next experimental steps in autonomous research system. Often, the accurate quantification of material parameters from experimental observables requires the inversion of a mathematical model that is used to approximate the physical reality of the experiment. As many models in physics are numerical solutions of (systems of) differential equations, such an inversion may often be impossible to do analytically. Instead, the comparison of the mathematical model with the experimental observable is often only possible by fitting the data using regression algorithms that solve the forward problem of

simulating the experiment often hundreds or thousands of times until they find a good agreement. In such situations, it is often unclear whether the found solution is correct or unique. Thus, despite an often quite time-consuming effort in data analysis, the predictive power of the result may be highly questionable.

A conceivable solution to this problem of fitting data in multidimensional parameter spaces is offered by the framework of Bayesian parameter inference that can be combined for instance with neural network based surrogate models as initially proposed in the context of photovoltaic research by Ren et al [18]. A decisive step in Bayesian inference is the definition of those material parameters that are allowed to vary to reproduce the experimental parameters. Those parameters will be the ones that the researcher conducting the study would classify as belonging to a class of parameters that either has a very high uncertainty (cannot independently be measured) and/or has a significant impact on the result. Parameters that are either well known or largely irrelevant would be excluded to reduce the dimensionality of the problem. This dimensionality reduction is currently often one of the least algorithmic parts of the process and it depends critically on the experience of the researchers involved in the study. In the so far quite limited literature on Bayesian inference in the context of photovoltaics, the initial step of determining which parameters to treat as free (high significance) and which to fix (low significance) has typically been approached in two ways. A common strategy is to incorporate insights from additional characterization techniques. For example, Hawks et al. [19] conducted photocurrent spectroscopy to understand the characteristics of defect states and include this information when fitting temperature-dependent current-voltage curves with drift-diffusion model. Similarly, Tang et al. [20] utilized various characterization tools to identify the cause of s-shaped current-voltage curves and include built-in voltage into one of free parameters to reproduce experimental data. Alternatively, some groups [21–23] rely on an extensive literature search on the material system of interest and fixed certain material parameters based on previously reported values. However, in many cases, the rationale behind parameter selection is not explicitly described or is partly explained (see **Table S1**), raising concerns regarding the justification of fitting and Bayesian inference process.

To judge, whether a certain set of free parameters in combination with a model is a useful (not necessarily correct) description of a physical reality, we have to discuss what “useful” would mean in this context. Generally, finding the material parameters of a semiconductor used in a functional (opto-)electronic device is useful if the combination of model and model-parameters have predictive power or if they can explain observed trends. Usually, the predictive power will be the stronger argument as it implies that the already known data is successfully described and in addition new data that the algorithm has not seen can be predicted. Here, we consider the classification of a model as useful to be more appropriate as opposed to correct, because usefulness can be quantified while correctness is nearly impossible to judge, when looking at experimental data.

Previously, we developed an approach based on a neural network (NN) model to extract material parameters θ such as mobilities and recombination coefficients from light-intensity-varied current-voltage (*JV*) curves [24]. With the constructed NN model at hand serving as a surrogate model for a drift-diffusion simulator, it is possible to extract best-fit parameters $\theta_{\text{best-fit}}$ within minutes. However, uncertainty may remain regarding the accuracy of the extracted parameters and whether the electro-optical model embedded in the NN truly reflects the charge transport dynamics in real solar cell systems.

To address this, predictive simulations using the inferred $\theta_{\text{best-fit}}$ can be compared against experimental data. For instance, using only two *JV* curves measured at different light intensities, one can extrapolate device performance across a broader illumination range to assess whether recombination losses are correctly captured. Furthermore, this kind of predictive modeling, once it is validated, is particularly valuable for organic photovoltaics, which are highly considered for indoor applications.

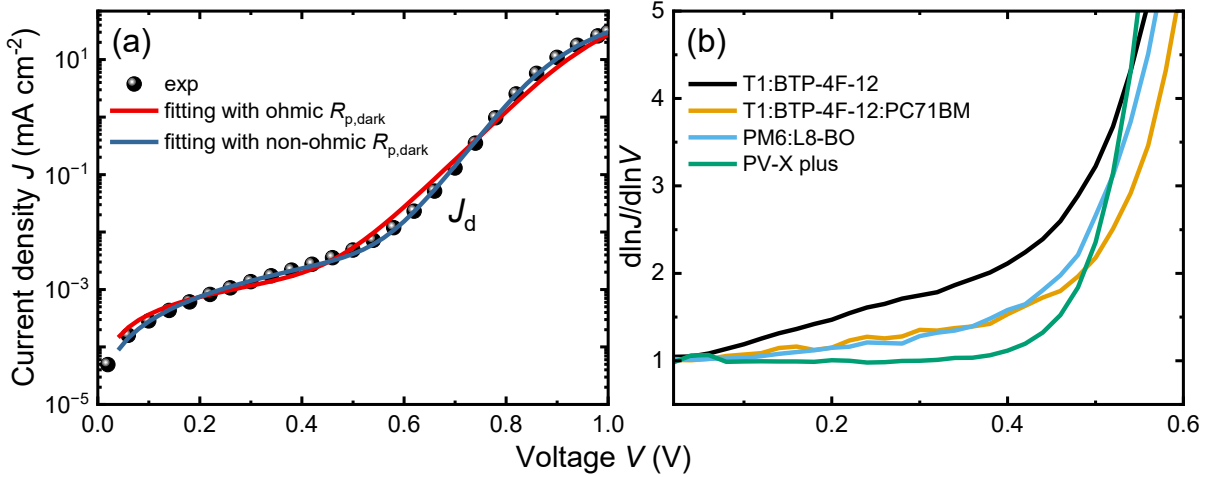


Figure 1. (a) Dark current-voltage curve of experimental data (dots) fitted using an equivalent circuit model with ohmic (red solid line) and non-ohmic (blue solid line) dark shunt resistance $R_{p,\text{dark}}$. (b) $d\ln J/d\ln V$ plotted against voltage for various absorber layer materials – T1:BTP-4F-12, T1:BTP-4F-12:PC71BM, PM6:L8-BO, and PV-X plus. The value of 1 indicates a linear relationship between current and voltage, while deviation from 1 suggests non-linear behavior.

The illuminated *JV* characteristics can be simply expressed as $J(V, \phi) = J_{\text{rec}}(V, \phi) - J_{\text{gen}}(\phi)$, where the current density is affected by the applied voltage V and the incident light intensity ϕ . The recombination current $J_{\text{rec}}(V, \phi)$, defined as the integral of recombination rate R over the absorber layer thickness, is influenced by factors such as the density of defect states, the strength of the recombination processes, and how fast the charges are extracted. Furthermore, the impact of this recombination mechanism on *JV* characteristics varies with light intensity, and these effects are reflected in parameters such as the mobility–lifetime product and the ideality factor n_{id} . At low light regime, the device performance is typically limited by defect-assisted recombination. However, when the dark shunt resistance $R_{p,\text{dark}}$ is sufficiently low, it becomes a dominant factor in determining efficiency [25–28]. It becomes the critical point for recombination losses that do not further decrease with reduced light intensity. Therefore, it is important to model the $R_{p,\text{dark}}$ accurately when fitting the illuminated *JV* curves. Conventionally, $R_{p,\text{dark}}$ is considered as an ohmic resistance [29–32]. In practice, however, it is often the case that the experimentally obtained dark *JVs* cannot be reconstructed with a linearly voltage-dependent $R_{p,\text{dark}}$ [33–37]. The nonlinear behavior of shunt resistance typically arises from the presence of pinholes in the absorber layer, providing alternative current path between the transport layers [34]. **Figure 1a** supports these findings, showing that incorporating a non-ohmic $R_{p,\text{dark}}$ results in a more accurate fit to the experimental data. Furthermore, **Figure 1b** illustrates the power coefficient α in the relation $J_{\text{d}} \propto V^\alpha$, where $\alpha > 1$ indicates non-ohmic behavior. Although the PV-X plus solution is likely to form homogeneous and pinhole-free films, most of the other material systems exhibits higher α values, suggesting nonlinear shunt behavior. Thus, verifying the presence of non-ohmic $R_{p,\text{dark}}$ is important for accurate prediction of device performance under low-light condition.

As light intensity increases, the influence of defect-assisted or bimolecular recombination becomes more significant. The extent to which the open-circuit voltage V_{oc} decreases with increasing light intensity depends on the dominant recombination mechanism. For example, if the recombination dominated by mid-gap trap states, the ideality factor n_{id} increases, leading to a steeper drop in V_{oc} with increasing light intensity, as described by $dV_{oc}/d\ln\phi \propto n_{id}$. At higher light intensity ($\phi \sim 1$ suns), series resistance predominantly reduces fill factor, causing voltage losses near V_{oc} . Unlike shunt resistance, incorporating series resistance into fitting procedures is challenging. Therefore, capturing n_{id} and the associated recombination coefficients or lifetime parameters is a key factor in understanding and predicting the light-intensity-dependent power conversion efficiency (PCE), particularly at high irradiance. In this regard, analyzing the JV curves in terms of shifted current density $J_{shifted} = J + J_{sc}$ can be especially useful to gain deeper insight into recombination dynamics. This shifted current is directly related to the recombination current ($J_{shifted}(V, \phi) = J_{rec}(V, \phi) - J_{rec}(V=0, \phi)$) and therefore encapsulates key information about recombination behavior, including the ideality factor and the mobility-lifetime product [26,38-40]. For example, $J_{shifted}$ exhibits a weak or even linear dependence on the voltage at small forward bias, where this effect is referred to as apparent shunt resistance $R_{p,photo}$. Unlike the dark shunt resistance, the $R_{p,photo}$ originates from nonzero charge carrier density or high quasi-Fermi-level splitting at short-circuit. It thus reflects the recombination dynamics and can serve as an indicator of the dominant recombination mechanism and order [39]. Therefore, directly fitting $J_{shifted}$ instead of the raw J could introduce more information in identifying material parameters in illumination-dependent JV data. Moreover, this approach allows separate treatment of J_{sc} , which is beneficial when calibration errors exist. Such errors, highlighted in discrepancies between experimentally measured and values calculated from external quantum efficiency EQE and light source spectra, can occur across different device compositions and light sources [41,42], and are unfortunately inconsistent. Furthermore, since the NN model is trained with a specific light spectrum, it is impractical to reconstruct the model each time a new device or illumination condition is introduced. Furthermore, this inconsistency can interfere with the accurate estimation of material parameters and limit the predictive capability of the model. In this regard, we could potentially resolve the EQE mismatch by adopting a sigmoid-like fitting function for J_{sc} .

To predict the light-intensity-dependent PCE, the dark JV curve is essential. It provides crucial information on the dark shunt resistance which is the dominant factor in recombination losses at low light regime. Moreover, it contains insights into the ideality factor, although it is predominantly influenced by the external parasitic resistances. Now, it would be interesting to investigate how many additional illuminated JV curves are required to reliably capture the light-intensity-dependent behavior of solar cells. Thus, in the following, we first perform Bayesian parameter estimation (BPE) using two JV curves measured at different light intensities and investigate how well the aforementioned device physics are reflected in the inferred material parameters. In this study, we adopt the BPE workflow established in previous literatures [24,43,44]. The material system discussed in the main text is T1:BTP-4F-12, with fabrication details provided in Supporting Information. Finally, we address an important question: how much and what type of JV data is necessary to accurately predict the light-intensity-dependent device performance? We compare the Bayesian inference results obtained from (i) a single dark JV , (ii) a dark JV and one light JV , and (iii) a dark JV and two light JVs . By analyzing the resulting

probability distributions of material parameters, we assess the information content of each dataset configuration and its impact on prediction accuracy.

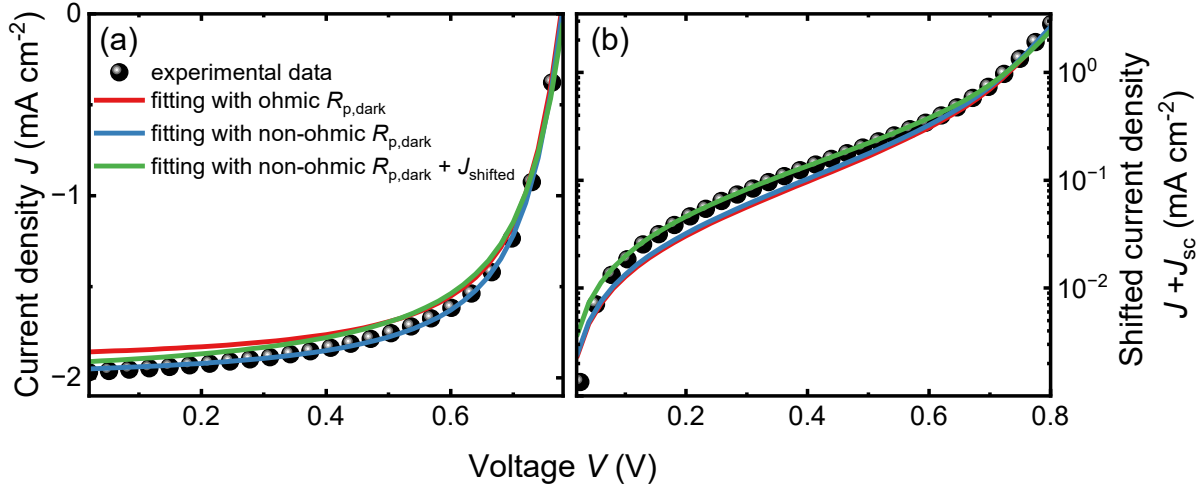


Figure 2. Current-voltage (JV) curves of experimental data used for fitting (dots) and the best-fit JV curves obtained under three types of condition (solid lines) at input light power density P_{in} of 5.5 mW cm^{-2} . The fitting using a pre-trained neural network model and CMA-ES genetic algorithm was conducted under the following conditions - assuming an ohmic $R_{p,\text{dark}}$ (red), a non-ohmic $R_{p,\text{dark}}$ (blue), and a non-ohmic $R_{p,\text{dark}}$ with increased weighting on the shifted JV ($J_{\text{shifted}} = J + J_{\text{sc}}$) compared to the short-circuit current J_{sc} (green).

The JV characteristics at light intensity of 5.5 and 72 mW cm^{-2} were simultaneously fitted using a pre-trained NN model and the CMA-ES genetic algorithm, followed by the identification of best-fit parameters $\theta_{\text{best-fit}}$. The NN model was originally constructed assuming an infinite dark shunt resistance ($R_{p,\text{dark}} = 10^{20} \Omega \text{m}^2$). Therefore, the external $R_{p,\text{dark}}$ – either ohmic or nonohmic – can be effortlessly incorporated during the fitting process without retraining the model. The incorporated first and second term of $R_{p,\text{dark}}$ are summarized in **Table S2**. As shown in **Figure 2a** (red and blue solid lines), including the non-ohmic $R_{p,\text{dark}}$ results in a better agreement to the experimental input, while the extracted $\theta_{\text{best-fit}}$ values are almost identical (**Table S3**). However, when visualized as J_{shifted} in logarithmic scale as shown in **Figure 2b**, there is still deviation from the experimental data even when non-ohmic $R_{p,\text{dark}}$ is incorporated. This discrepancy is likely due to imperfect calibration of the white LED lamp used for measurement, leading to inconsistent mismatches $J_{\text{sc,measured}}/J_{\text{sc,EQE}}$ at different light intensities. To address this, we modified the fitting approach by directly fitting J_{shifted} and separately fitting the J_{sc} with reduced weight. (see Supporting Information) This strategy enabled an excellent fit to the shifted JV curves (green and blue solid lines in **Figure 2b**), while there is bigger error at original scale.

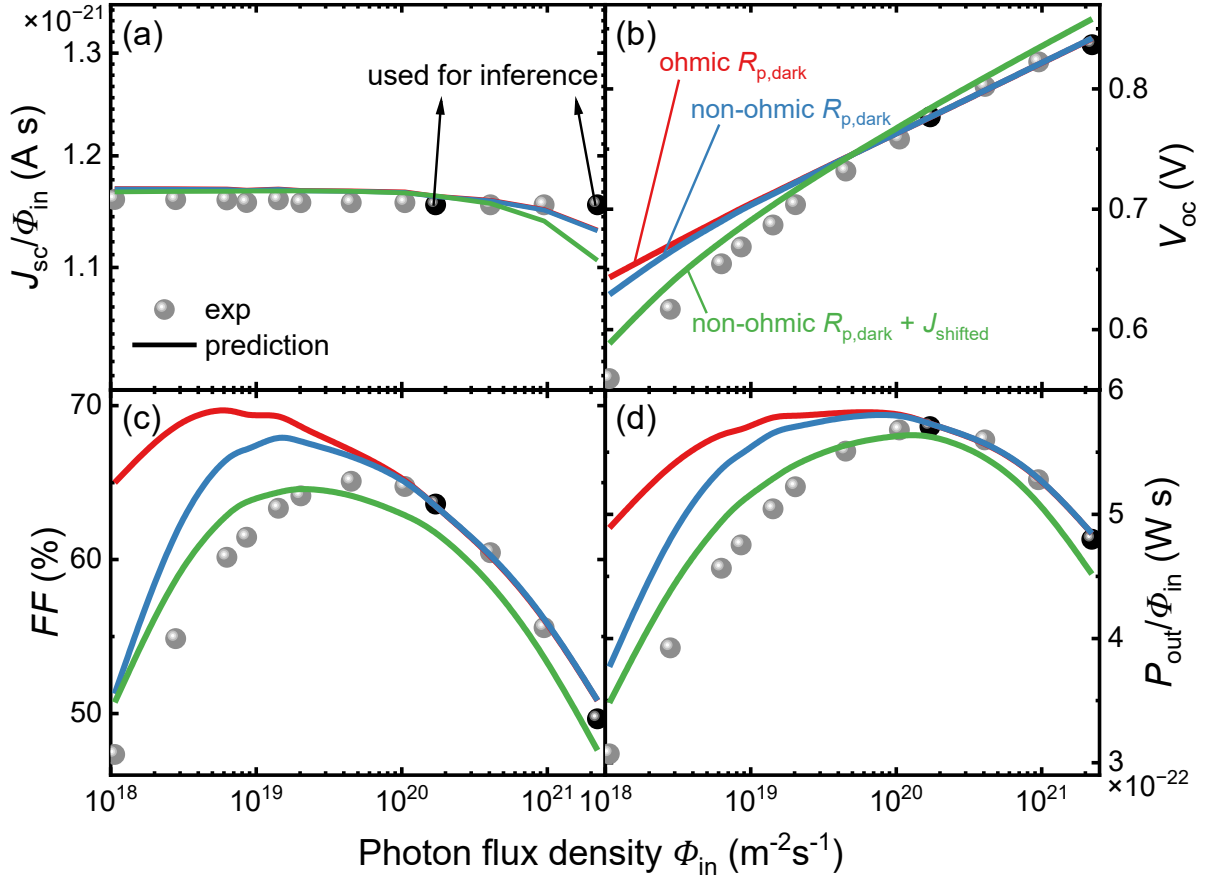


Figure 3. Solar cell parameters of illumination-dependent current-voltage (JV) characteristics obtained from PBDB-TF-T1:BTP-4F-12 solar cells (grey dots) and predicted JV characteristics with the extracted best-fit parameters under three different fitting conditions (solid lines): (a) short-circuit current density normalized by the input power density J_{sc}/P_{in} , (b) open-circuit voltage V_{oc} , (c) fill factor FF , and (d) efficiency. The experimental data used for parameter inference is highlighted with the black color. The fitting was conducted under the following conditions - assuming an ohmic $R_{p,dark}$ (red), a non-ohmic $R_{p,dark}$ (blue), and a non-ohmic $R_{p,dark}$ with increased weighting on the shifted JV ($J_{shifted} = J + J_{sc}$) compared to the short-circuit current J_{sc} (green).

Figure 3 compares the device performance between the experimental data and the predictions using the inferred $\theta_{best-fit}$ under three different fitting conditions. While the predicted short-circuit current densities J_{sc} consistently deviate from the experimental data, partly due to changes in the optical filter during LED measurements [26], the prediction accuracy for FF is significantly improved when a nonohmic $R_{p,dark}$ is incorporated, particularly at low light regime. This highlights the value of dark JV data in predicting device performance in the low light intensity regime. However, discrepancies between the predicted and experimental data still remain under low and intermediate illumination levels. Furthermore, parameters extracted from the shifted JV curves result in decreased FF and V_{oc} , leading to better agreement with experimental data, though they exhibit reduced accuracy in J_{sc} . The improvement in prediction accuracy can be attributed to more reliable estimation of material parameters by adjusting the μ , N_{dt} , and k_{dir} values (Table S3). Particularly, the defect density exhibited the largest variation when the $J_{shifted}$ is highlighted during fitting procedure. A higher N_{dt} value of $2.9 \times 10^{15} \text{ cm}^{-3}$ compared to $4.18 \times 10^{14} \text{ cm}^{-3}$ obtained from the fitting with JV at original scale emphasizes the influence of defect-assisted recombination at low and intermediate light intensity regime, leading to better prediction for FF and V_{oc} . On the other hand, the device performance predictions at higher light intensities deviates

from the experimental data, likely due to the influence of dark series resistance, which is not fully accounted for in the current workflow.

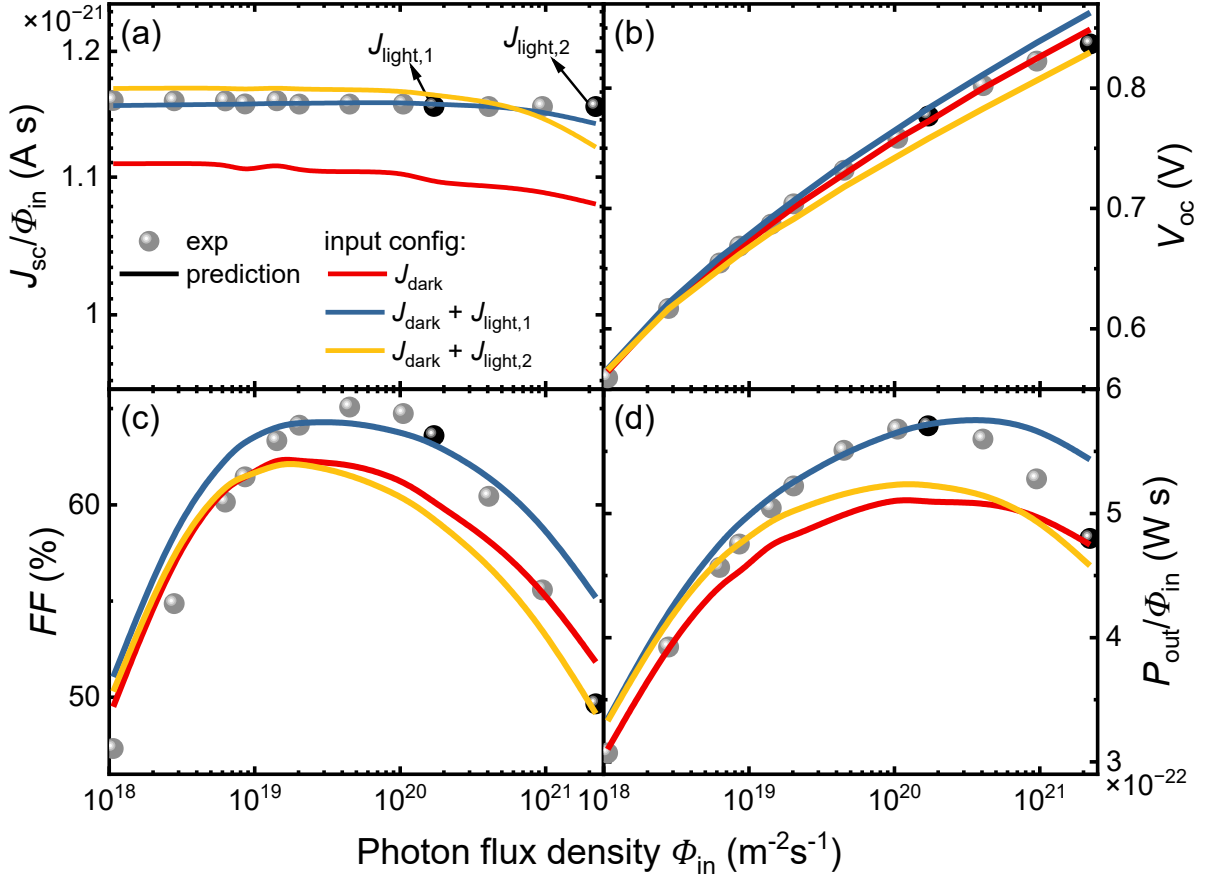


Figure 4. Solar cell parameters of illumination-dependent current-voltage (*JV*) characteristics obtained from PBDB-TF-T1:BTP-4F-12 solar cells (grey dots) and predicted *JV* characteristics with the extracted best-fit parameters from various combinations of input dataset (solid lines): (a) open-circuit voltage V_{oc} and (b) fill factor FF . The illuminated *JV* curves used for Bayesian inference are highlighted in black color and labelled as $J_{light,1}$ and $J_{light,2}$. (c-e) Projected multivariate probability densities onto one-dimensional space for mobility μ , defect density N_{dt} , and direction recombination coefficient k_{dir} , obtained from parameter estimation using three different types of input dataset – a single dark *JV* curve (red), one dark and one light *JV* curve (blue), and two light *JV* curves (green).

In this last part, we aim to understand the information content of *JV* curves measured under different light intensities and in the dark. Accordingly, we conducted parameter inference using various combinations of input data – a single dark *JV*, and combinations of one dark *JV* and a light *JV* measured either at 5.5 mW cm^{-2} (denoted as $J_{light,1}$) or 72 mW cm^{-2} ($J_{light,2}$), while the corresponding prediction results are illustrated in **Figure 4a** and **4b**. Interestingly, using only the dark *JV* curve for inference results in reasonably accurate predictions of V_{oc} , while the FF is not well captured, particularly under intermediate illumination levels. Once an illuminated *JV* curve $J_{light,1}$ is incorporated, the FF predictions improve significantly. However, when the light *JV* at high intensity ($J_{light,2}$) is used in combination with the dark *JV*, the prediction accuracy decreases. This inaccuracy can be attributed to the increasing influence of series resistance at higher light intensities which are not included in NN model. Consequently, the recombination losses that should be ascribed to the series resistance are instead misattributed to a higher direction recombination coefficient (**Table S4**), leading to misleading parameter inference. On the other hand, poor prediction accuracy using only dark *JV* curve likely stems from its limited information content. For example, exciton dissociation probability which eventually

determines the photogenerated charge carrier density cannot be extracted from dark *JV* data alone. While J_{dark} contains information about recombination dynamics such as saturation current, it lacks insights into how the quasi-fermi-level splitting evolves under illumination. This results in slight deviations in the inferred values of mobility and direct recombination coefficient (**Table S4**), ultimately degrading the accuracy of light-intensity-dependent performance predictions. The uncertainty of parameter estimation is further visualized in the probability distribution plots for key electronic parameters (**Figure 4c-e**). When a single J_{dark} is used, the distributions are relatively uniform and have no clear peaks, indicating high uncertainty. In contrast, the inclusion of a light *JV* curve produces distinct peaks in the distributions, enabling more confident and accurate parameter estimation. As information content of the dataset J_{dark} and J_{light} is comparable to that of two light *JV* curves, the input configuration of J_{dark} and J_{light} at low or intermediate light intensities (to minimize the influence of series resistance) is sufficient to accurately capture the light-intensity-dependent behavior of solar cells.

While the machine learning techniques enable efficient estimation of material parameters using a neural network (NN) surrogate mode, the reliability of the inferred parameters depends on hidden assumptions such as the choice of the one-dimensional drift-diffusion model, the reduction of the parameter space to six variables, and the underlying physical representations embedded in the NN model. Therefore, validating the extracted parameters through predictive modelling is an important step. It is a well-established principle that the dark shunt resistance $R_{\text{p,dark}}$ limits the device performance at low light intensities, while at intermediate and high intensities the charge carriers recombination become critical. We confirmed that these physical trends were reflected in our workflow of Bayesian parameter estimation and prediction of light-intensity-dependent *JV* characteristics using the best-fit parameters $\theta_{\text{best-fit}}$. The prediction accuracy for open-circuit voltage V_{oc} and fill factor FF is significantly improved when the $R_{\text{p,dark}}$ was correctly modelled, particularly at low light regime. This additionally highlights the value of dark *JV* data. However, deviations between prediction and experimental data remain prominently in the shifted current density ($J_{\text{shifted}} = J + J_{\text{sc}}$), which is highly sensitive to recombination losses such as mobility-lifetime product or ideality factors. Placing greater emphasis on fitting J_{shifted} resulted in enhanced accuracy in predicting V_{oc} and FF at low to intermediate light intensities. Finally, by comparing different input data configurations, we identified which combinations of *JV* curves contain sufficient information to reproduce the full light-intensity-dependent device behavior. While using only a dark *JV* curve yields reasonable predictions given the limited data, it lacks information on photogenerated carrier behavior, resulting in lower accuracy. Incorporating at least one light *JV* curve significantly improves prediction reliability. However, one should be careful when choosing which light *JV* to include since if it is measured at high light intensity, there could be an influence from series resistance, leading to inaccurate parameter estimation.

Reference

- [1] J. M. Granda, L. Donina, V. Dragone, D.-L. Long, L. Cronin, *Nature* **2018**, *559*, 377.
- [2] J. Li, J. Li, R. Liu, Y. Tu, Y. Li, J. Cheng, T. He, X. Zhu, *Nat Commun* **2020**, *11*, 2046.
- [3] K. Abdel-Latif, R. W. Epps, F. Bateni, S. Han, K. G. Reyes, M. Abolhasani, *Advanced Intelligent Systems* **2021**, *3*, 2000245.
- [4] H. Tao, T. Wu, S. Kheiri, M. Aldeghi, A. Aspuru-Guzik, E. Kumacheva, *Advanced Functional Materials* **2021**, *31*, 2106725.
- [5] K. Higgins, M. Ziatdinov, S. V. Kalinin, M. Ahmadi, *J. Am. Chem. Soc.* **2021**, *143*, 19945.

- [6] T. C. Wu, A. Aguilar-Granda, K. Hotta, S. A. Yazdani, R. Pollice, J. Vestfrid, H. Hao, C. Lavigne, M. Seifrid, N. Angello, F. Bencheikh, J. E. Hein, M. Burke, C. Adachi, A. Aspuru-Guzik, *Advanced Materials* **2023**, *35*, 2207070.
- [7] J. Wu, L. Torresi, M. Hu, P. Reiser, J. Zhang, J. S. Rocha-Ortiz, L. Wang, Z. Xie, K. Zhang, B. Park, A. Barabash, Y. Zhao, J. Luo, Y. Wang, L. Lüer, L.-L. Deng, J. A. Hauch, D. M. Guldi, M. E. Pérez-Ojeda, S. I. Seok, P. Friederich, C. J. Brabec, *Science* **2024**, *386*, 1256.
- [8] C. Kunkel, F. Rüther, F. Felsen, C. W. P. Pare, A. Terzi, R. Baumgarten, E. Gioria, R. Naumann d'Alnoncourt, C. Scheurer, F. Rosowski, K. Reuter, *ACS Catal.* **2024**, *14*, 9008.
- [9] H. J. Yoo, N. Kim, H. Lee, D. Kim, L. T. C. Ow, H. Nam, C. Kim, S. Y. Lee, K.-Y. Lee, D. Kim, S. S. Han, *Advanced Functional Materials* **2024**, *34*, 2312561.
- [10] M. Ismail, M. Angeles Cabañero, J. Orive, L. Musuvadhi Babulal, J. Garcia, M. C. Morant-Miñana, J.-L. Dauvergne, F. Bonilla, I. Monterrubio, J. Carrasco, A. Saracibar, M. Reynaud, *Digital Discovery* **2025**, *4*, 943.
- [11] S. Langner, F. Häse, J. D. Perea, T. Stubhan, J. Hauch, L. M. Roch, T. Heumueller, A. Aspuru-Guzik, C. J. Brabec, *Advanced Materials* **2020**, *32*, 1907801.
- [12] J. Zhang, B. Liu, Z. Liu, J. Wu, S. Arnold, H. Shi, T. Osterrieder, J. A. Hauch, Z. Wu, J. Luo, J. Wagner, C. G. Berger, T. Stubhan, F. Schmitt, K. Zhang, M. Sytnyk, T. Heumueller, C. M. Sutter-Fella, I. M. Peters, Y. Zhao, C. J. Brabec, *Advanced Energy Materials* **2023**, *13*, 2302594.
- [13] C. C. Rupnow, B. P. MacLeod, M. Mokhtari, K. Ocean, K. E. Dettelbach, D. Lin, F. G. L. Parlante, H. N. Chiu, M. B. Rooney, C. E. B. Waizenegger, E. I. de Hoog, A. Soni, C. P. Berlinguette, *CR-PHYS-SC* **2023**, *4*.
- [14] N. Meftahi, M. A. Surmiak, S. O. Fürer, K. J. Rietwyk, J. Lu, S. R. Raga, C. Evans, M. Michalska, H. Deng, D. P. McMeekin, T. Alan, D. Vak, A. S. R. Chesman, A. J. Christofferson, D. A. Winkler, U. Bach, S. P. Russo, *Advanced Energy Materials* **2023**, *13*, 2203859.
- [15] M. Hußner, R. A. Pacalaj, G. Olaf Müller-Dieckert, C. Liu, Z. Zhou, N. Majeed, S. Greedy, I. Ramirez, N. Li, S. M. Hosseini, C. Uhrich, C. J. Brabec, J. R. Durrant, C. Deibel, R. C. I. MacKenzie, *Advanced Energy Materials* **2024**, *14*, 2303000.
- [16] E. B. Miftahullatif, S. D. Pethe, A. K. Y. Low, A. A. Zhumekenov, N. Yantara, P. Kajal, Q. Wu, D. J. Jie Tay, D. Sharma, S. Sebastian, J. Recatala-Gomez, N. Abhishek, N. Mathews, K. Hippalgaonkar, *ACS Energy Lett.* **2025**, *10*, 3952.
- [17] C. Wang, Y.-J. Kim, A. Vriza, R. Batra, A. Baskaran, N. Shan, N. Li, P. Darancet, L. Ward, Y. Liu, M. K. Y. Chan, S. K. R. S. Sankaranarayanan, H. C. Fry, C. S. Miller, H. Chan, J. Xu, *Nat Commun* **2025**, *16*, 1498.
- [18] Z. Ren, F. Oviedo, M. Thway, S. I. P. Tian, Y. Wang, H. Xue, J. Dario Perea, M. Layurova, T. Heumueller, E. Birgersson, A. G. Aberle, C. J. Brabec, R. Stangl, Q. Li, S. Sun, F. Lin, I. M. Peters, T. Buonassisi, *npj Comput Mater* **2020**, *6*, 9.
- [19] S. A. Hawks, G. Li, Y. Yang, R. A. Street, *J. Appl. Phys.* **2014**, *116*, 074503.
- [20] Z. Tang, J. Wang, A. Melianas, Y. Wu, R. Kroon, W. Li, W. Ma, M. R. Andersson, Z. Ma, W. Cai, W. Tress, O. Inganäs, *J. Mater. Chem. A* **2018**, *6*, 12574.
- [21] T. Golubev, D. Liu, R. Lunt, P. Duxbury, *AIP Advances* **2019**, *9*, 035026.
- [22] A. Riquelme, L. J. Bennett, N. E. Courtier, M. J. Wolf, L. Contreras-Bernal, A. B. Walker, G. Richardson, J. A. Anta, *Nanoscale* **2020**, *12*, 17385.
- [23] X. Zhao, C. Huang, E. Birgersson, N. Suprun, H. Q. Tan, Y. Zhang, Y. Jiang, C. Shou, J. Sun, J. Peng, H. Xue, *Applied Energy* **2025**, *392*, 125922.
- [24] E. Kim, P. Hartnagel, B. Urbano, L. Christen, T. Kirchartz, *Solar RRL* *n/a*, e202500648.
- [25] R. Steim, T. Ameri, P. Schilinsky, C. Waldauf, G. Dennler, M. Scharber, C. J. Brabec, *Solar Energy Materials and Solar Cells* **2011**, *95*, 3256.
- [26] D. Lübke, P. Hartnagel, M. Hülsbeck, T. Kirchartz, *ACS Mater. Au* **2023**, *3*, 215.
- [27] C. M. Proctor, T.-Q. Nguyen, *Appl. Phys. Lett.* **2015**, *106*, 083301.
- [28] G. Burwell, O. J. Sandberg, W. Li, P. Meredith, M. Carnie, A. Armin, *Solar RRL* **2022**, *6*, 2200315.
- [29] W. Tress, In *Organic Solar Cells: Theory, Experiment, and Device Simulation* (Ed.: Tress, W.), Springer International Publishing, Cham, **2014**, pp. 67–214.
- [30] J. Nelson, *The Physics Of Solar Cells*, World Scientific Publishing Company, **2003**.
- [31] N. M. Mangan, R. E. Brandt, V. Steinmann, R. Jaramillo, C. Yang, J. R. Poindexter, R. Chakraborty, H. H. Park, X. Zhao, R. G. Gordon, T. Buonassisi, *J. Appl. Phys.* **2015**, *118*, 115102.

- [32] T. Kirchartz, K. Ding, U. Rau, In *Advanced Characterization Techniques for Thin Film Solar Cells*, John Wiley & Sons, Ltd, **2016**, pp. 41–69.
- [33] S. Dongaonkar, J. D. Servaites, G. M. Ford, S. Loser, J. Moore, R. M. Gelfand, H. Mohseni, H. W. Hillhouse, R. Agrawal, M. A. Ratner, T. J. Marks, M. S. Lundstrom, M. A. Alam, *J. Appl. Phys.* **2010**, *108*, 124509.
- [34] P. Kaienburg, P. Hartnagel, B. E. Pieters, J. Yu, D. Grabowski, Z. Liu, J. Haddad, U. Rau, T. Kirchartz, *J. Phys. Chem. C* **2018**, *122*, 27263.
- [35] T. J. McMahon, T. J. Berniard, D. S. Albin, *J. Appl. Phys.* **2005**, *97*, 054503.
- [36] T. R. Johnson, G. Ganguly, G. S. Wood, D. E. Carlson, *MRS Online Proceedings Library* **2011**, *762*, 77.
- [37] O. Kunz, J. Wong, J. Janssens, J. Bauer, O. Breitenstein, A. g. Aberle, *Progress in Photovoltaics: Research and Applications* **2009**, *17*, 35.
- [38] D. Grabowski, Z. Liu, G. Schöpe, U. Rau, T. Kirchartz, *Solar RRL* **2022**, *6*, 2200507.
- [39] E. Kim, L. Christen, T. Kirchartz, *Advanced Energy Materials* *n/a*, 2403129.
- [40] C. Wang, R. C. I. MacKenzie, U. Würfel, D. Neher, T. Kirchartz, C. Deibel, M. Saladina, *Advanced Energy Materials* *n/a*, 2405889.
- [41] E. Zimmermann, P. Ehrenreich, T. Pfadler, J. A. Dorman, J. Weickert, L. Schmidt-Mende, *Nature Photon* **2014**, *8*, 669.
- [42] M. Saliba, E. Unger, L. Etgar, J. Luo, T. J. Jacobsson, *Nat Commun* **2023**, *14*, 5445.